Multimode coupled flutter and buffeting analysis of long span bridges

Xinzhong Chen[a], Ahsan Kareem[a],*, Masaru Matsumoto[b]

[a] *Department of Civil Engineering and Geological Sciences, University of Notre Dame, 163 Fitzpatrick, Notre Dame, IN 46556-0767, USA*
[b] *Department of Global Environment Engineering, Kyoto University, Kyoto 606-8501, Japan*

Abstract

In this paper, the equations of structural motion are expressed in time-invariant state-space equations by expressing the frequency dependent self-excited forces in terms of rational functions. Accordingly, the multimode coupled flutter analysis is reduced to evaluate the eigenvalues of a constant matrix at each prescribed wind velocity. This formulation is computationally efficient in comparison with the conventional iterative approach. The complex mode approach is utilized for analyzing efficiently the coupled buffeting response. This approach is computationally more efficient than the conventional scheme in which a matrix inversion is required to evaluate the system transfer function at each frequency. A long span cable-stayed bridge and a suspension bridge are used to investigate the coupled flutter. The effect of the aerodynamic coupling among modes on the buffeting response is ascertained and compared to conventional mode-by-mode approach. © 2001 Elsevier Science Ltd. All rights reserved.

Keywords: Flutter; Buffeting; Random vibration; Complex mode analysis; Bridges; State space; Linear system

1. Introduction

The flutter and buffeting response analysis of long span bridges exposed to turbulent wind excitation is generally performed in the frequency domain based on the approach originally proposed by Davenport [1] and Scanlan [2,3]. For many bridges, the flutter response is generally dominated by a single torsional uncoupled

*Corresponding author. Tel.: +1-219-631-5380; fax: +1-219-631-9236.
E-mail address: kareem@nd.edu (A. Kareem).

mode, and the flutter frequency is very close to the natural frequency. The primary effect of the self-excited forces is to change the structural damping through the aerodynamic damping. Both the aerodynamic and structural coupling among modes are neglected in the conventional approach for the estimation of aerodynamic damping and the modal buffeting response. These modal response components are then summed using the square root of sum of squares (SRSS) approach for estimating the total response.

For an aerodynamically tailored bridge deck section with a typical span length, the torsional flutter which is dominated by a single torsional mode can be eliminated or postponed to higher wind velocity. For very long span bridges, the coupled flutter caused by the coupling among the self-excited forces in the vertical and torsional directions may become a critical problem. In fact, an increase in bridge span length results in a significant decrease in the natural frequency and in the ratio between the first symmetric torsional and vertical frequencies. This lends itself to a need to examine coupled flutter at higher range of reduced wind velocity to ensure a wind resistant design [4]. Not only the coupled flutter instability needs to be avoided, but also the buffeting response needs to be evaluated at wind velocities near the critical flutter velocity. In this case, conventional simplified procedures for multimode response may become invalid, and the aerodynamic coupling between modal responses must be considered for an accurate estimation of flutter and buffeting response [5–9]. Recent advances in the coupled buffeting and flutter analyses of long span bridges can be found from Refs. [10,11,8,9].

The multi-mode coupled flutter analysis is commonly performed through a solution of a nonlinear complex eigenvalue problem [5]. Since the unsteady self-excited forces are a function of reduced frequency, each solution associated to each mode needs an iterative calculation until the assumed frequency coincides with that of the prescribed target mode. This procedure can be time consuming and computationally cumbersome particularly for multi-mode flutter analysis of long span bridges that have closely-spaced frequencies. The computational efficiency of the flutter analysis can be improved by representing the unsteady self-excited forces in terms of a rational function approximation [8]. Further examination of the contribution of each self-excited force component to the system damping would aid in improving our understanding of the flutter generation mechanism [8]. The mode-by-mode approach for predicting the buffeting response, in which the aerodynamic coupling among modes are neglected, may lead to an underestimation of the response of long span bridges at high wind velocities [8]. An accurate estimation of response requires a precise prediction of the aerodynamic damping and proper consideration of the changes that take place in mode shapes due to aerodynamic coupling.

In this paper, the equations of structural motion are described in terms of time-invariant state-space equations by expressing the frequency dependent self-excited forces in terms of rational functions. Accordingly, the multimode coupled flutter analysis is reduced to the determination of the eigenvalues of a constant matrix at each prescribed wind velocity. Similarly, the coupled buffeting analysis can be conducted efficiently by utilizing the complex mode approach. The effectiveness of

the analysis procedure outlined here is demonstrated by evaluating the coupled multimode flutter response of a long span cable-stayed bridge and a suspension bridge. The effect of the aerodynamic coupling among various modes on the buffeting response is addressed and compared to conventional mode-by-mode approach.

2. Theoretical background

2.1. Equations of motion

The dynamic response of a bridge exposed to turbulent wind in the vertical, lateral and torsional directions $h(x, t)$, $p(x, t)$ and $\alpha(x, t)$ are expressed in terms of the generalized coordinates $\mathbf{q} = \{q_j\}$ as

$$h(x, t) = \sum_j h_j(x)q_j(t), \quad p(x, t) = \sum_j p_j(x)q_j(t), \quad \alpha(x, t) = \sum_j \alpha_j(x)q_j(t) \qquad (1)$$

where $h_j(x)$, $p_j(x)$ and $\alpha_j(x)$ are the jth mode shapes in the vertical, lateral and torsional directions, respectively.

The governing equations of motion in modal coordinates are given by

$$\mathbf{M}\ddot{\mathbf{q}} + \mathbf{C}\dot{\mathbf{q}} + \mathbf{K}\mathbf{q} = \mathbf{Q}_{\mathrm{se}} + \mathbf{Q}_{\mathrm{b}} \qquad (2)$$

where $\mathbf{M}, \mathbf{C}, \mathbf{K}$ are the generalized mass, damping and stiffness matrices, respectively; $\mathbf{Q}_{\mathrm{se}}$ and $\mathbf{Q}_{\mathrm{b}}$ are the generalized self-excited and buffeting force vectors, respectively; and the over-dot denotes partial differentiation with respect to time.

The self-excited and buffeting force components per unit length, i.e. lift (downward), drag (downwind) and pitching moment (nose-up) are expressed as

$$L_{\mathrm{se}}(t) = \frac{1}{2}\rho U^2 (2b) \left(kH_1^* \frac{\dot{h}}{U} + kH_2^* \frac{b\dot{\alpha}}{U} + k^2 H_3^* \alpha + k^2 H_4^* \frac{h}{b} \right.$$
$$\left. + kH_5^* \frac{\dot{p}}{U} + k^2 H_6^* \frac{p}{b} \right) \qquad (3)$$

$$D_{\mathrm{se}}(t) = \frac{1}{2}\rho U^2 (2b) \left(kP_1^* \frac{\dot{p}}{U} + kP_2^* \frac{b\dot{\alpha}}{U} + k^2 P_3^* \alpha + k^2 P_4^* \frac{p}{b} + kP_5^* \frac{\dot{h}}{U} + k^2 P_6^* \frac{h}{b} \right) \qquad (4)$$

$$M_{\mathrm{se}}(t) = \frac{1}{2}\rho U^2 (2b^2) \left(kA_1^* \frac{\dot{h}}{U} + kA_2^* \frac{b\dot{\alpha}}{U} + k^2 A_3^* \alpha + k^2 A_4^* \frac{h}{b} \right.$$
$$\left. + kA_5^* \frac{\dot{p}}{U} + k^2 A_6^* \frac{p}{b} \right) \qquad (5)$$

$$L_{\mathrm{b}}(t) = -\frac{1}{2}\rho U^2 (2b) \left[2C_L \chi_{Lu} \frac{u(t)}{U} + (C_L' + C_D)\chi_{Lw} \frac{w(t)}{U} \right] \qquad (6)$$

$$D_{\mathrm{b}}(t) = \frac{1}{2}\rho U^2(2b)\left[2C_D\chi_{Du}\frac{u(t)}{U} + (C'_D - C_L)\chi_{Dw}\frac{w(t)}{U}\right] \tag{7}$$

$$M_{\mathrm{b}}(t) = \frac{1}{2}\rho U^2(2b)^2\left[2C_M\chi_{Mu}\frac{u(t)}{U} + C'_M\chi_{Mw}\frac{w(t)}{U}\right] \tag{8}$$

where ρ is the air density, U is the mean wind velocity, $B = 2b$ is the bridge deck width, $k = \omega b/U$ is the reduced frequency, ω is the circular frequency, H_i^*, P_i^* and A_i^* ($i = 1 \sim 6$) are the flutter derivatives, χ_{Lu}, χ_{Lw}, χ_{Du}, χ_{Dw}, χ_{Mu} and χ_{Mw} are the aerodynamic admittance functions, C_D, C_L, C_M are the static coefficients; $C'_L = \mathrm{d}C_L/\mathrm{d}\alpha$ and $C'_M = \mathrm{d}C_M/\mathrm{d}\alpha$, u and w are the longitudinal and vertical wind fluctuations, respectively, and subscripts se and b designate the self-excited and buffeting components, respectively.

Based on the finite element discretization, $\mathbf{Q}_{\mathrm{se}}$ and $\mathbf{Q}_{\mathrm{b}}$ can be determined as functions of the bridge flutter derivatives, the aerodynamic admittance functions, the spanwise correlation functions of the buffeting forces, and the mode shapes. These can be expressed in terms of the generalized coordinates and the wind fluctuation vectors as given below:

$$\mathbf{Q}_{\mathrm{se}} = \frac{1}{2}\rho U^2\left(\mathbf{A}_s(\mathrm{i}k)\mathbf{q} + \frac{b}{U}\mathbf{A}_d(\mathrm{i}k)\dot{\mathbf{q}}\right) \tag{9}$$

$$\mathbf{Q}_{\mathrm{b}} = \frac{1}{2}\rho U^2\left(\mathbf{A}_{bu}(\mathrm{i}k)\frac{\mathbf{u}}{U} + \mathbf{A}_{bw}(\mathrm{i}k)\frac{\mathbf{w}}{U}\right) \tag{10}$$

The self-excited forces corresponding to the steady-state motion $\mathbf{q}(t) = \bar{\mathbf{q}}\,\mathrm{e}^{\mathrm{i}\omega t}$ can be approximated in terms of a rational function [12],

$$\begin{aligned}
\mathbf{Q}_{\mathrm{se}}(t) &= \tfrac{1}{2}\rho U^2(\mathbf{A}_s + (\mathrm{i}k)\mathbf{A}_d)\bar{\mathbf{q}}\,\mathrm{e}^{\mathrm{i}\omega t}\\
&= \tfrac{1}{2}\rho U^2\left(\mathbf{A}_1 + (\mathrm{i}k)\mathbf{A}_2 + (\mathrm{i}k)^2\mathbf{A}_3 + \sum_{l=1}^{m}\frac{(\mathrm{i}k)\mathbf{A}_{l+3}}{\mathrm{i}k + d_l}\right)\bar{\mathbf{q}}\,\mathrm{e}^{\mathrm{i}\omega t}
\end{aligned} \tag{11}$$

where $\mathbf{A}_1$, $\mathbf{A}_2$, $\mathbf{A}_3$, $\mathbf{A}_{l+3}$ and d_l ($d_l \geqslant 0$; $l = 1 \sim m$) are the frequency independent matrices and parameter. This approximation due to Roger [12] can be determined by fitting the experimentally obtained data of $\mathbf{A}_s(\mathrm{i}k)$ and $\mathbf{A}_d(\mathrm{i}k)$ defined at a set of discretized reduced velocities k_j ($j = 1, 2, \ldots$) using a least-square approach.

Employing the concept of analytic continuation, similar expression can be given for arbitrary motion $\mathbf{q}(t) = \bar{q}\,\mathrm{e}^{st}$ with $\bar{s} = sb/U = (-\xi + \mathrm{i})k$ substituted for $\mathrm{i}k$ in Eq. (11), where $s = (-\xi + \mathrm{i})\omega$ and ξ is the damping ratio.

After some manipulations, the equations of motion can be expressed as frequency independent linear time-invariant state-space equations:

$$\dot{\mathbf{Y}}(t) = \mathbf{A}\mathbf{Y}(t) + \mathbf{B}\mathbf{Q}_{\mathrm{b}}(t) \tag{12}$$

where

$$\mathbf{A} = \begin{bmatrix} \mathbf{0} & \mathbf{I} & \mathbf{0} & \ldots & \mathbf{0} \\ -\bar{\mathbf{M}}^{-1}\bar{\mathbf{K}} & -\bar{\mathbf{M}}^{-1}\bar{\mathbf{C}} & \frac{1}{2}\rho U^2\bar{\mathbf{M}}^{-1} & \ldots & \frac{1}{2}\rho U^2\bar{\mathbf{M}}^{-1} \\ \mathbf{0} & \mathbf{A}_4 & -\frac{U}{b}d_1\mathbf{I} & \ldots & \mathbf{0} \\ \vdots & \vdots & \vdots & & \vdots \\ \mathbf{0} & \mathbf{A}_{3+m} & \mathbf{0} & \ldots & -\frac{U}{b}d_m\mathbf{I} \end{bmatrix} \tag{13}$$

$$\mathbf{Y} = \begin{bmatrix} \mathbf{q} \\ \dot{\mathbf{q}} \\ \mathbf{q}_{se1} \\ \vdots \\ \mathbf{q}_{sem} \end{bmatrix}, \quad \mathbf{B} = \begin{bmatrix} \mathbf{0} \\ \bar{\mathbf{M}}^{-1} \\ \mathbf{0} \\ \vdots \\ \mathbf{0} \end{bmatrix} \tag{14}$$

where $\bar{\mathbf{M}} = \mathbf{M} - \frac{1}{2}\rho b^2\mathbf{A}_3$, $\bar{\mathbf{C}} = \mathbf{C} - \frac{1}{2}\rho Ub\mathbf{A}_2$, $\bar{\mathbf{K}} = \mathbf{K} - \frac{1}{2}\rho U^2\mathbf{A}_1$, $\mathbf{q}_{sel}$ $(l = 1 \sim m)$ are the introduced new vectors representing the unsteady aerodynamic states.

It is noted that if the self-excited forces can be represented exactly or with an acceptable error by a rational function of the reduced frequency k or dimensionless Laplace variable $\bar{s}$ (Eq. (11)), Eq. (2) leads to a rigorous interpretation in the state space (Eq. (12)), which provides significant mathematical advantages. For flutter analysis, by utilizing Eq. (12), the nonlinear eigenvalue analysis of Eq. (2) can be replaced by the determination of the eigenvalues of a constant matrix $\mathbf{A}$ at each prescribed wind velocity. Note that the nonlinear eigenvalue problem is quite cumbersome, especially in the case of multi-mode coupled flutter of very long span bridges. Comparing to the flutter analysis based on the eigenvalue analysis at prescribed reduced velocity, analysis at prescribed wind velocity provides information of how the eigen-properties of a bridge are influenced by the interaction of the bridge and wind with the change in wind velocity. This is also convenient for comparison with wind tunnel tests utilizing full aeroelastic models. The results predicted at a specific wind velocity are also useful for the analysis of buffeting response in both frequency and time domains. Eq. (12) facilitates an efficacious time domain analysis of systems with frequency-dependent self-excited forces. This feature is quite appealing as it can expedite the Monte Carlo simulation of the system. The recasting of the equations of motion in the state-space format allows the use of tools based on the linear system theory for the analysis and control of dynamic response.

2.2. Multimode flutter analysis

The flutter analysis is conducted by omitting the buffeting forces and finding the solution of a complex eigenvalue problem of linear time-invariant state-space

equations (Eq. (12)). Using the complex modal analysis and solving the eigenvalue problem leads to N conjugate pairs of complex eigenvalue and eigenvectors (where N is the natural mode number included), which correspond to structural modes, and $m * N$ negative real eigenvalues and real eigenvectors (where m is the order of rational function approximation), which correspond to the additional aerodynamic states introduced by the rational function approximations. The eigenvalues corresponding to structural modes can be expressed as

$$\lambda_j = -\xi_j \omega_j + i\omega_j \sqrt{1 - \xi_j^2}, \quad (j = 1, \dots, N) \tag{15}$$

The eigenvalues at different wind velocities provide insight into the changes in frequencies and damping ratios with an increase in wind velocity. The eigenvectors indicate the aerodynamic coupling among natural modes due to the self-excited forces. The system is stable when all of the eigenvalues lie to the left side of the imaginary axis in the complex plane. When one of the eigenvalues has a zero real part, it means the flutter occurrence and this wind velocity is referred to as the critical flutter velocity.

At the critical flutter velocity, the free vibration can be expressed as

$$\mathbf{Z}(t) = \boldsymbol{\Psi}(\boldsymbol{\Phi}_r \, e^{\lambda_r t} + \boldsymbol{\Phi}_r^* \, e^{\lambda_r^* t}) \tag{16}$$

where $\mathbf{Z}$ is the physical coordinates, $\boldsymbol{\Psi}$ the mode shape matrix, $\boldsymbol{\Phi}_r$ the rth complex eigenvector corresponding to the modal displacement of flutter mode, and superscript $*$ denotes the complex conjugate operator.

2.3. Buffeting response analysis

Based on random vibration theory, the power spectral density matrix of the generalized modal coordinates $\mathbf{q}$ and the physical coordinates $\mathbf{Z}$ are given by

$$\mathbf{S}_q(i\omega) = \mathbf{H}(i\omega)\mathbf{S}_{Qb}(i\omega)\mathbf{H}(-i\omega)^T, \tag{17}$$

$$\mathbf{S}_Z(i\omega) = \boldsymbol{\Psi}\mathbf{S}_q\boldsymbol{\Psi}^T \tag{18}$$

where $\mathbf{S}_{Qb}(i\omega)$ is the power spectral density matrix of the generalized buffeting forces, $\boldsymbol{\Psi}$ the modal shape matrix, and $\mathbf{H}(i\omega)$ the transfer matrix including the effects of the self-excited forces

$$\mathbf{H}(i\omega) = \left[-\omega^2 \mathbf{M} + i\omega \left(\mathbf{C} - \frac{1}{2}\rho U b \mathbf{A}_d \right) + \left(\mathbf{K} - \frac{1}{2}\rho U^2 \mathbf{A}_s \right) \right]^{-1} \tag{19}$$

It is emphasized that Eqs. (17) and (18) gives the complete coupling form that includes both structural and aerodynamic coupling effects, which are indicated by the non-zero off-diagonal components of $\mathbf{S}_{Qb}(i\omega)$, and $\mathbf{H}_q(i\omega)$, respectively. Neglecting these coupling effects leads to the conventional simplified SRSS approach.

Most current technique involve direct calculation of $\mathbf{H}(i\omega)$ from Eq. (19), which requires an inverse of the matrix at every frequency within the range of interest [13]. When results are needed for only a limited number of frequencies, the overall time

required for direct calculation may be shorter, but it will be very time consuming when large number of modes and a fine frequency discretization is required for accuracy. The following approach based on the complex mode analysis provides improvement in computational efficiency [14].

Normalizing the distinct eigenvector Γ_j corresponding to the eigenvalues λ_j ($j = 1, \ldots, n$; $n = (2 + m)N$) and defining the $n*n$ matrix $\boldsymbol{\Gamma}$ by

$$\Gamma_j^{\mathrm{T}}\Gamma_j = 1, \quad \boldsymbol{\Gamma} = [\Gamma_1, \Gamma_2, \ldots, \Gamma_n] \tag{20}$$

and

$$\boldsymbol{\Gamma}^{-1}\mathbf{A}\boldsymbol{\Gamma} = \Lambda, \quad \Lambda = \mathrm{diag}[\lambda_1, \ldots, \lambda_n] \tag{21}$$

Now the transfer function $\mathbf{H}(\mathrm{i}\omega)$ is given by

$$\mathbf{H}(\mathrm{i}\omega) = \mathbf{D}(\mathrm{i}\omega\mathbf{I} - \mathbf{A})^{-1}\mathbf{B} = \mathbf{D}\boldsymbol{\Gamma}(\mathrm{i}\omega\mathbf{I} - \Lambda)^{-1}\boldsymbol{\Gamma}^{-1}\mathbf{B} \tag{22}$$

where matrix $\mathbf{D}$ is defined by

$$\mathbf{q} = \mathbf{D}\mathbf{Y}, \quad \mathbf{D} = [\mathbf{I}, \mathbf{0}, \ldots, \mathbf{0}] \tag{23}$$

It is noted that for the evaluation of the transfer matrix at a prescribed wind velocity, only the complex eigenvalue analysis and the inversion of the eigenvector matrix are required once, and the matrix inversion is not needed at each frequency. This leads to computational efficiency in comparison with the conventional scheme. It is also worth pointing out that the stochastic decomposition technique offers another computationally efficient procedure to calculate the power spectral density of the buffeting response [15]. The root-mean-square (RMS) values of the buffeting responses are then calculated from the integrations of its power spectral density.

The buffeting analysis based on complex mode analysis has also been conducted by Cremona et al. [16] and Yamada et al. [17]. In the former paper, based on the assumption that the mode frequencies are well separated and the transfer function of a particular mode can be approximated through the aerodynamic matrices ($\mathbf{A}_s$ and $\mathbf{A}_d$) defined at the corresponding peak frequency, a simplified approach has been proposed for buffeting analysis. In Ref. [17], the buffeting response of the complex mode coordinates has been calculated through the power spectral density analysis, which needs more computational effort than the traditional practice based on the real structural modal coordinates. The scheme proposed in the present paper is considered to be computationally more efficient and can be applied to multi-mode coupled buffeting analysis.

The von Karman spectra for u and w components are used in this study for describing the power spectra of the wind fluctuations. Based on the field observation that even as the frequency goes to zero, the coherence is not necessarily unity, the following coherence function is utilized for the evaluation of joint acceptance for the consideration of buffeting forces reduction due to spanwise correlation:

$$\mathrm{coh}_r(\Delta x, f) = \exp\left(-\frac{0.747|\Delta x|}{2\pi L_r^x}\sqrt{1 + 70.78\left(\frac{fL_r^x}{U}\right)^2}\right) \tag{24}$$

where r indicates the u- and w-components; L_r^x is the integral scales in the along-wind direction; λ_r is the decay factor, and Δx is the distance of the points in the across-wind direction.

The admittance functions for drag, lift and moment components are based on the functions given by Davenport and the Sears function, respectively.

$$|\chi|_D^2 = \frac{2}{k_1^2}[k_1 - 1 + \exp(-k_1)] \tag{25}$$

$$|\chi|_{LM}^2 = \frac{a + k}{a + (\pi a + 1)k + 2\pi k^2} \tag{26}$$

where $\chi_D = \chi_{Du} = \chi_{Dw}$, $k_1 = \lambda f D/U$, λ is the decay factor, D the height of bridge deck, $\chi_{LM} = \chi_{Lu} = \chi_{Lw} = \chi_{Mu} = \chi_{Mw}$, $k = \omega b/U$, and $a = 0.1811$.

3. Numerical examples and analysis

A cable-stayed bridge and a suspension bridge with center spans of about 1000 and 2000 m, respectively, are used as examples. The logarithmic decrement for each mode is assumed to be 0.02. Details concerning other structural parameters are omitted for brevity. For the sake of illustrating the fundamental characteristics of flutter and buffeting response, only the aerodynamic forces acting on the bridge deck are included. For very long span cable-stayed bridges, wind loading on stay cables must be included for accurate response analysis. Considering that the emphasis of this study is on the aerodynamic coupling effects rather than the structural coupling, the contribution of loading on cables and the structural coupling between cables, towers and deck are not included in this study. The self-excited drag component induced by the lateral motion is represented by the quasi-steady theory. The self-excited lift and moment components induced by the lateral motion and the self-excited drag components induced by the vertical and torsional motions are generally negligible and are neglected here. For the cable-stayed bridge, the flutter derivatives H_i^* and A_i^* ($i = 1,2,3,4$) are calculated from the Theodorsen function. For the suspension bridge, in addition to the flutter derivatives based on the Theodorsen function, experimental results from a twin-box section are also used for comparison [18]. These two bridge sections are identified as Sections 1 and 2, respectively, in the subsequent discussion. In Fig. 1, some of the flutter derivatives are presented for these sections.

Various combinations of the natural modes are considered in the calculation of multimode coupled flutter to investigate the natural mode participation. For the cable-stayed bridge, the predicted flutter condition is summarized in Table 1, in which modes 3, 6 and 11 are the first, second and third symmetric vertical bending modes, mode 10 is the second symmetric lateral bending mode and mode 13 the first symmetric torsional mode. Figs. 2 and 3 show the changes in the frequency and damping ratio as the wind velocity is increased. Table 2 shows the changes in the
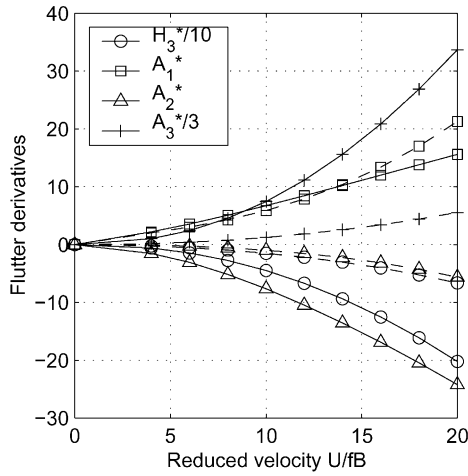
Fig. 1. Flutter derivatives ((−) Section 1; (− −) Section 2).

Table 1
Flutter conditions (cable-stayed bridge)

Mode no.	Branch	Velocity (m/s)	Frequency (Hz)
3,13	mode 13	119.3	0.3583
3,10	mode 10	175.2	0.4111
3,6,13	mode 13	118.4	0.3661
3,6,10,11,13	mode 10	114.3	0.3495
1–20	mode 10	113.8	0.3506
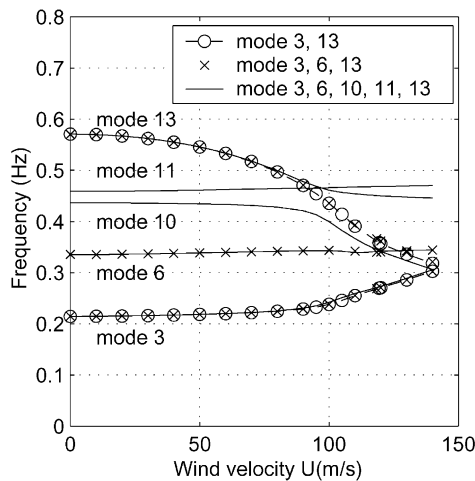
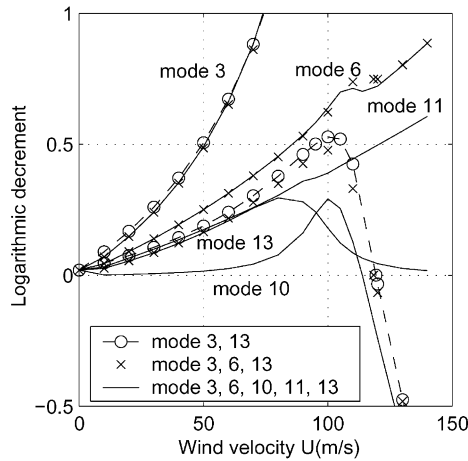Fig. 2. Frequency versus wind velocity (cable-stayed bridge).

Fig. 3. Damping ratio versus wind velocity (cable-stayed bridge).

Table 2
Magnitude of natural mode (cable-stayed bridge)

Mode no.	3	10	13	3	10	13
U(m/s)	Complex mode 10			Complex mode 13		
60.0	0.11	**1.00**	0.10	0.23	0.10	**1.00**
80.0	0.29	**1.00**	0.27	0.40	0.26	**1.00**
100.0	1.43	**1.00**	0.99	0.69	0.95	**1.00**
113.2	2.82	0.62	**1.00**	0.48	**1.00**	0.62
120.0	3.36	0.57	**1.00**	0.42	**1.00**	0.52

magnitude of each natural mode in the complex modes 10 and 13. It is noted that although the genesis of flutter seems to follow a different path when different mode combinations are considered, they are all physically consistent. The properties of the complex modes 10 and 13 have been switched when their frequencies become close at the wind velocity around 110 m/s.

For the suspension bridge example, the predicted frequency and damping ratio of each mode for both sections with different mode combinations are presented in Figs. 4–7. The predicted flutter conditions are summarized in Table 3, in which modes 2 and 8 are the first and second symmetric vertical bending modes, mode 9 is the second symmetric lateral bending mode and mode 10 the first symmetric torsional mode. In the case of Section 1, similar to the cable-stayed bridge, the complex modes 9 and 10 switch their properties at the wind velocity of about 60 m/s (Table 4). In the case of Section 2, both favorable uncoupled self-excited force components (i.e. the components corresponding to A_2^* and A_3^*) and unfavorable
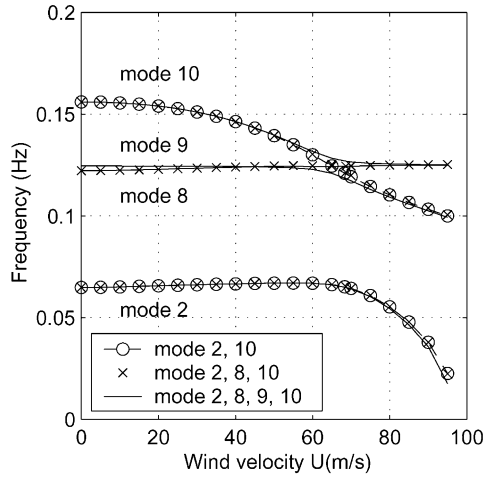
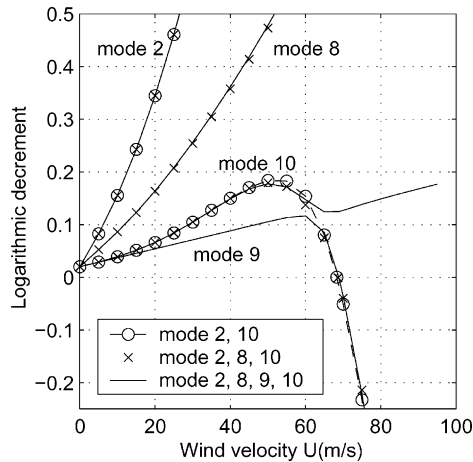Fig. 4. Frequency versus wind velocity (suspension bridge, Section 1).

Fig. 5. Damping ratio versus wind velocity (suspension bridge, Section 1).

coupled force components (i.e. the component corresponding to H_3^*) are less than those calculated from the Theodorsen function. These features of the self-excited forces result in insignificant changes in the damping ratio of the flutter mode (complex mode 10) as the wind velocity increases. In general, uncoupled self-excited forces result in an increase in the system damping, but the coupled self-excited forces result in a decrease in the system damping [8]. Therefore, it is important to reduce the unfavorable contributions of the coupled self-excited forces and to increase the favorable contributions of the uncoupled self-excited forces for improving the
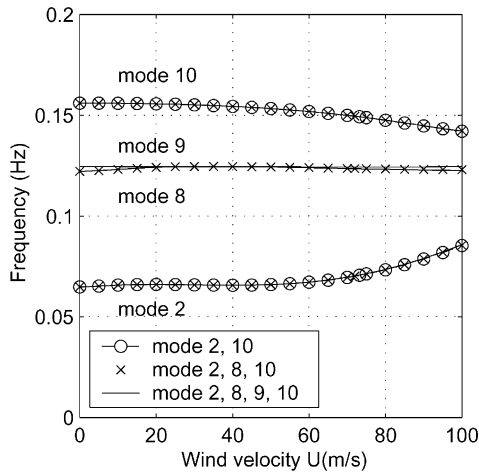
Fig. 6. Frequency versus wind velocity (suspension bridge, Section 2).
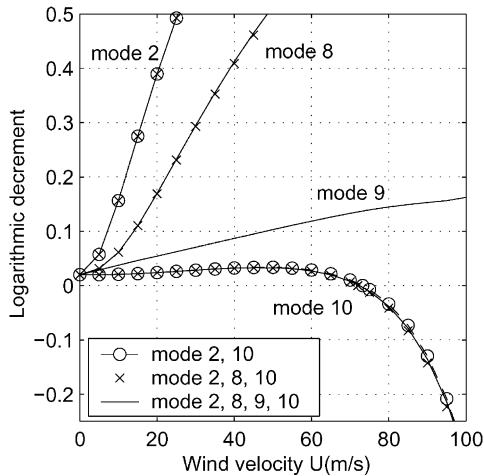

Fig. 7. Damping ratio versus wind velocity (suspension bridge, Section 2).

overall performance of a bridge experiencing coupled flutter. This can be realized by the structural and aerodynamic modifications of the structural system and the geometric configuration of the bridge deck.

Detailed investigations on the amplitude of the complex modes and the contribution of each self-excited force component to the system damping are important for improving understanding of the mechanism responsible for coupled

Table 3
Flutter conditions (suspension bridge)

Mode no.	Branch	Velocity (m/s)	Frequency (Hz)
Section 1: based on Theodorsen function			
2,10	mode 10	68.3	0.1210
2,8,10	mode 10	68.6	0.1214
2,8,9,10	mode 9	68.9	0.1181
1–15	mode 9	69.3	0.1186
Section 2: two-box section			
2,10	mode 10	73.2	0.1492
2,8,10	mode 10	72.0	0.1495
2,8,9,10	mode 10	72.4	0.1494
1–15	mode 10	74.8	0.1484

flutter. In both examples, the analysis including only the fundamental vertical bending and torsional modes can provide results very close to those obtained by considering higher modes. It may be in part due to the significant changes in the flutter mode damping ratio as the wind velocity increases, thus a marginal contribution from the higher modes to the system damping results in a little change in the flutter onset velocity. For this hard-type flutter case, some structural control devices such as TMD/ATMD added to increase the structural damping to postpone flutter instability may not be effective. On the contrary, the soft-type flutter may be apparently influenced by the higher modes and also be more amendable to control by structural and/or aerodynamic means.

In the multi-mode coupled buffeting analysis, for the suspension bridge with Section 2, the first 15 natural modes are considered. The spanwise correlation of buffeting forces are assumed to be the same as those of the wind fluctuations. The length scale and turbulence intensity in along wind and across wind directions are assumed to be 80 and 40 m, and 10% and 5%, respectively. The following three cases are considered: (a) complete coupling, i.e. $H_{qij} \neq 0$ and $S_{Qbij} \neq 0$ $(i \neq j)$, (b) with aerodynamic coupling but ignoring the structural coupling, i.e. $H_{qij} \neq 0$ but $S_{Qbij} = 0$ $(i \neq j)$, (c) conventional mode-by-mode analysis and a subsequent combination using SRSS approach, i.e. $H_{qij} = 0$ and $S_{Qbij} = 0$ $(i \neq j)$.

In Fig. 8, the RMS torsional responses at the center of main span at different wind velocities are presented. Fig. 9 shows the response along the bridge axis at the wind velocity of 70 m/s. Results indicate that at higher wind velocity, the buffeting response is significantly underestimated in the vertical and torsional directions when the aerodynamic coupling effects are neglected, although the buffeting response in lateral direction is not apparently affected by the aerodynamic coupling. The structural coupling due to the correlation between the generalized buffeting forces show only a very little influence on the vertical buffeting response.

Table 4
Magnitude of natural mode (suspension bridge, Section 1)

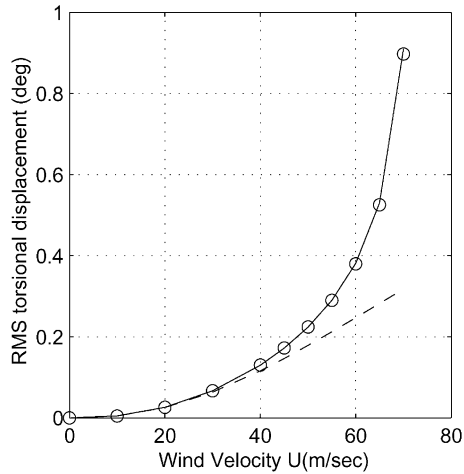| Mode no.	2	8	9	10	2	8	9	10
U(m/s)	Complex mode 9				Complex mode 10			
40.0	0.05	0.15	**1.00**	0.05	0.23	0.10	0.07	**1.00**
60.0	0.43	0.44	**1.00**	0.37	0.73	0.51	0.49	**1.00**
68.9	1.50	0.70	0.77	**1.00**	0.57	0.25	**1.00**	0.59
80.0	2.29	0.51	0.39	**1.00**	0.27	0.04	**1.00**	0.26

Fig. 8. RMS torsional response at the center of main span versus wind velocity ((−) complete coupling; (o) w/o structural coupling; (− −) w/o aerodynamic and structural coupling).

4. Concluding remarks

A new scheme for the coupled flutter and buffeting analysis has been presented which is based on the complex mode analysis of a linear time-invariant system. In this analysis the unsteady frequency dependent aerodynamic wind forces are recast in terms of rational function approximation which results in frequency independent force description.

Results have indicated that the aerodynamic coupling between the natural modes particularly between the fundamental vertical bending and torsional modes is most significant for the coupled flutter.

Neglecting the aerodynamic coupling results in a significant under prediction of the buffeting response in the vertical and torsional directions at wind velocities near the critical flutter velocity. Furthermore, the structural coupling due to the correlation between the generalized buffeting forces show only a very little influence on the vertical buffeting response.
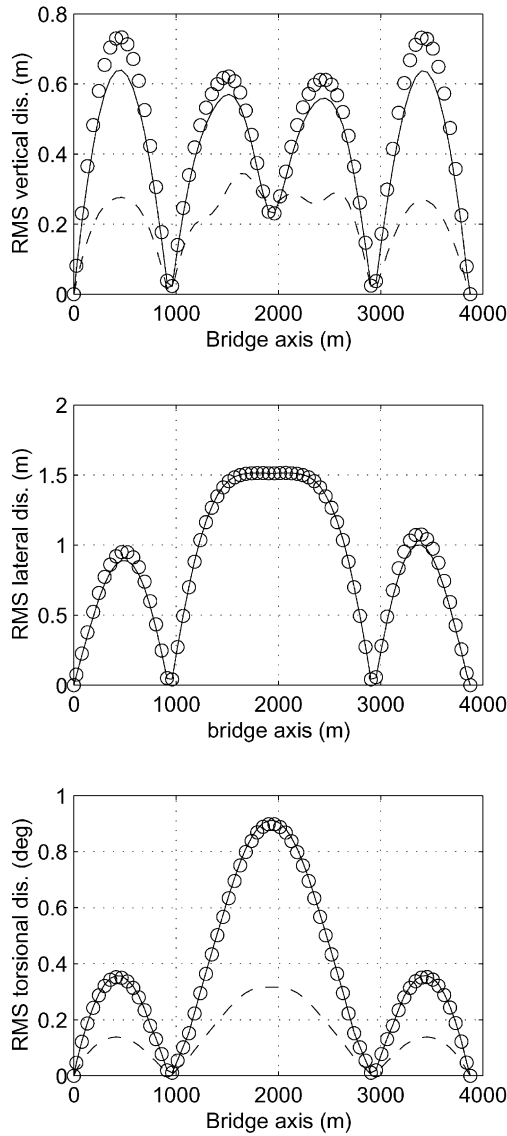
Fig. 9. RMS response along the span at wind velocity of 70 m/s ((−) complete coupling; (o) w/o structural coupling; (− −) w/o aerodynamic and structural coupling).

Acknowledgements

Laboratory, University of Notre Dame, Notre Dame, IN, for his comments on the manuscript.

References

[1] A.G. Davenport, Buffeting of a suspension bridge by storm winds, J. Struct. Eng. Division ASCE 88 (ST6) (1962) 233–264.

[2] R.H. Scanlan, The action of flexible bridges under wind, I: flutter theory, J. Sound Vibration 60 (2) (1978) 187–199.

[3] R.H. Scanlan, The action of flexible bridges under wind, II: buffeting theory, J. Sound Vibration 60 (2) (1978) 201–211.

[4] T. Miyata, K. Tada, H. Sato, H. Katsuchi, Y. Hikami, New findings of coupled flutter in full model wind tunnel tests on the Akashi Kaikyo Bridge, Proceedings of the Symposium on Cable-Stayed and Suspension Bridges, Deauville, France, October 12–15, 1994, pp. 163–170.

[5] T.T.A. Agar, Aerodynamic flutter analysis of suspension bridges by a modal technique, Eng. Struct. 11 (1989) 75–82.

[6] A. Jain, N.P. Jones, R.H. Scanlan, Coupled flutter and buffeting analysis of long-span bridges, J. Struct. Eng. ASCE 122 (7) (1996) 716–725.

[7] H. Katsuchi, N.P. Jones, R.H. Scanlan, Multimode coupled flutter and buffeting analysis of the Akashi-Kaikyo Bridge, J. Struct. Eng. ASCE 125 (1999) 60–70.

[8] X. Chen, M. Matsumoto, A. Kareem, Aerodynamic coupling effects on flutter and buffeting of bridges, J. Eng. Mech. ASCE 126 (1) (2000) 17–26.

[9] X. Chen, M. Matsumoto, A. Kareem, Time domain flutter and buffeting response analysis of bridges, J. Eng. Mech. ASCE 126 (1) (2000) 7–16.

[10] N.P. Jones, R.H. Scanlan, A. Jain, H. Katsuchi, Advances (and challenges) in the prediction of long-span bridge response to wind, in: Larsen, Esdahl (Eds.), Bridge Aerodynamics, A.A. Balkema, Rotterdam, 1998, pp. 59–85.

[11] G. Diana, S. Bruni, A. Collina, A. Zasso, Aerodynamic challenges in super long span bridges design, in: Larsen, Esdahl (Eds.), Bridge Aerodynamics, A.A. Balkema, Rotterdam, 1998, pp. 131–144.

[12] K.L. Roger, Airplane math modeling methods for active control design, AGARO-CP-228, 1977.

[13] A. Kareem, Wind effects on structures: a probabilistic viewpoint, Probabilistic Eng. Mech. 2 (4) (1987) 166–200.

[14] T.T. Soong, M. Grigoriu, Random vibration of mechanical and structural systems, Prentice-Hall, Englewood Cliffs, NJ, 1993.

[15] Y. Li, A. Kareem, Stochastic decomposition and application to probabilistic dynamics, J. Eng. Mech. 121 (1) (1995) 162–174.

[16] C. Cremona, A.P. Solares, Simplified approach for assessing bridge buffeting response with aeroelastic interaction. Proceedings of the Second East European Conference on Wind Engineering, Prague, 1998, pp. 89–96.

[17] H. Yamada, T. Miyata, N.N. Minh, H. Katsuchi, Complex flutter-mode analysis for coupled gust response of the Akashi Kaikyo Bridge model, in: Larose, Livesey (Eds.), Wind Engineering into 21st Century, A.A. Balkema, Rotterdam, 1999, pp. 1081–1088.

[18] M. Matsumoto, T. Yagi, H. Ishizaki, H. Shirato, X. Chen, Aerodynamic stability of 2-edge girders for cable-stayed bridge, Proceedings of the 15th National Symposium on Wind Engineering, JAWE, 1998, pp. 389–394 (in Japanese).